International Journal for Housing Science and Its Applications
Publish August 4, 2025. Volume 46, Issue 3 Pages 2697-2705

https://doi.org/10.70517/ijhsa463227

Micromechanical and morphological analysis of the role of inclusions in the tensile fracture behavior of U26Mn2Si2CrNiMo bainitic austenitic steel

Shibo Liu[1,*] and Zhiqing Chen[2]
[1] School of Materials Science and Engineering, Shenyang Aerospace University, Shenyang, Liaoning, 110000, China
[2] School of Management, Chongqing University of Technology, Chongqing, 400054, China
Corresponding authors: (e-mail: liushibo200010@163.com).

Abstract This study takes U26Mn2Si2CrNiMo bainitic austenitic steel as the object, and systematically investigates the micromechanical role and morphological evolution mechanism of inclusions in its tensile fracture behavior. The influence of the cooling process on the organization evolution is analyzed by establishing a temperature field model, and the variation rule of mechanical properties is revealed by combining room temperature and low temperature tensile experiments. The microstructural features are characterized by multi-scale microscopic techniques such as metallurgical microscopy, scanning electron microscopy and transmission electron microscopy. The results show that the normalizing final cooling temperature affects the distribution of grain boundary mismatch angle and residual austenite by regulating the degree of bainite phase transformation, which in turn changes the material toughness and toughness, and the full austenite organization is realized under the final cooling condition of 320℃. The La element addition caused the average size of inclusions to decrease and then increase, with H1, H2, and H3 varying to 0.62 μm, 0.43 μm, and 0.49 μm. The material strength and plasticity are synergistically enhanced under low-temperature tensile conditions, and the pulse current treatment reduces the work-hardening capacity through softening effect. This paper provides a theoretical basis for the control of inclusions and process optimization of steel for railroad turnout heart rails.

Index Terms U26Mn2Si2CrNiMo, tensile fracture behavior, temperature field model, mechanical properties, low temperature stretching

I. Introduction

Accompanying the process of China's industrialization and modernization, the iron and steel industry, as a basic industry, provides a large amount of raw material support for the modernization of the country [1]. The industrial status quo of China's de-capacity and the extreme demand for key high-end steel materials make the research and development of high-performance steel materials particularly critical [2]. Rational design, optimization of existing steel materials heat treatment process and through the simulation of the composition and process design to shorten the research and development cycle, saving research costs so that the steel materials in the higher strength while ensuring good toughness has become a new generation of steel materials of basic research is the most important [3]-[6].

Bainitic steel has excellent strength, toughness and adequate wear resistance and other comprehensive mechanical properties, and easier to weld with high-carbon steel, which in the field of railroad transportation and other areas show a high potential for application [7], [8]. Bainitic steels are mainly used to improve their mechanical properties by optimizing the alloying elements and optimizing the heat treatment process in two ways [9]. In China, Tsinghua University developed a high-strength Mn-Si-Cr bainitic austenitic steel with a strength of 1500 MPa in 2002 [10]. Mn-Si-Cr bainitic steels can obtain high strength under air-cooling conditions without adding expensive alloying elements in the composition, which results in low alloying cost [11], [12]. At the same time, the air-cooling process is simple and does not require special cooling equipment, which can save the production cost of bainitic steels, and it is easy to realize industrialized mass production [13], [14]. However, the special and extreme service conditions put forward higher requirements on the comprehensive performance of steel materials, which should not only have high strength, but also ensure good toughness [15], [16]. Therefore, by observing and analyzing the crack expansion during tensile fracture of existing bainitic steels of Mn-Si-Cr system, it is of great significance for expanding their application areas and increasing the service safety and reliability [17]-[19].

In this paper, the temperature field of strip steel after fast cooling in the presence of latent heat of phase change is considered, and mechanical property tests are designed for both room temperature and low temperature conditions. The microstructure evolution of the samples in different states is observed using various characterization means such as metallurgical microscopy, X-ray diffraction, scanning electron microscopy, electron backscatter diffraction, and transmission electron microscopy. Simulate the temperature distribution and organization transformation during the cooling process, and analyze the regulation of the normalizing final cooling temperature on the bainite phase transformation and residual austenite. The correlation between inclusions and fracture toughness is established by using multi-dimensional microstructure characterization. Combined with room temperature and low temperature tensile experiments, we quantify the strong plasticity and work-hardening behavior of the material, and investigate the effect of pulsed current treatment on the fracture mechanism.

II. Mechanical property analysis and morphological characterization of materials under temperature field modeling

Railroad traffic as an important form of transportation in China, the railroad turnout rut and is the key equipment for track change, and the heart rail is the key component of the railroad turnout rutting fork, its mechanical properties stability and safety of railroad transportation is closely related. Due to the bainitic steel has excellent strength, toughness and sufficient wear resistance and other comprehensive mechanical properties, and easier to weld with high carbon steel, its application in the rut and the heart of the rail on the prospect of attracting widespread attention.

Austenitic steel is mainly through the strengthening of heterogeneous nuclei to refine its solidification organization, inclusions as a nucleus plasma efficiency and its and austenitic organization between the point mismatch degree related, nucleus plasma the more the number of points, the more obvious the effect of refinement. However, coarse inclusions may become a source of cracks, leading to fracture of the weld metal, so the research focuses on the type, quantity and size control of inclusions to further optimize the mechanical properties of the weld metal. However, the micromechanical behavior of inclusions under dynamic loading and their coupling mechanism with microstructure have not been clarified. In this paper, a systematic study is carried out around material property testing and structural characterization, aiming at revealing the key role of inclusions in tensile fracture and providing theoretical support for optimizing the material process.

II. A. Cooling process temperature field model

II. A. 1) Calculation of the temperature field

The general actual production length of strip steel is more than 800m, the thickness is 0.8~2.2mm, and the width is about 800mm. In the heat exchange process after cooling, the heat flow in the length direction can generally be ignored, and only the transverse and thickness directions are considered. Considering the release of latent heat in the phase change process, the two-dimensional thermal conductivity differential equation of strip steel containing an internal heat source is used, and the mathematical model of the temperature field established is as follows:

$$\frac{\partial}{\partial x}\left(\lambda\frac{\partial T}{\partial x}\right)+\frac{\partial}{\partial y}\left(\lambda\frac{\partial T}{\partial y}\right)+Q=\rho c\left(\frac{\partial T}{\partial t}\right) \quad (1)$$

where λ is the thermal conductivity of the steel, W/m·°C; ρ is the density of the steel, kg/m³Q is the rate of thermal conductivity for the heat source within the strip, J/s; t is the time, s; c is the specific heat capacity of the material, J/(kg·K); and x, y is the value of the strip's transverse and thickness-direction coordinates, m respectively.

II. A. 2) Initial and boundary conditions

The initial and boundary conditions are given by the following equations:

$$T(x,y,t)=T(x,y,0) \quad (2)$$

$$\lambda\left(\frac{\partial T}{\partial x}lx+\frac{\partial T}{\partial y}ly\right)+H(Tr-Ta)=0 \quad (3)$$

where x, y is the value of the right-angle coordinate in the transverse and thickness directions; lx, ly is the unit vector of the right-angle coordinate in the transverse and thickness directions; H is the coefficient of heat exchange, W/m²·℃; Tr, Ta is the surface temperature of the strip and the ambient temperature, respectively.

II. A. 3) Differential Method for Calculating the Temperature Field

In this paper, the explicit finite difference method is used to solve the partial differential equation of thermal conductivity. The explicit difference has the advantages of simple structure and can be solved directly without the need of joint equations, but the step size in space and time need to have corresponding constraints to ensure the convergence stability of the equations.

Where the constraint equation after discretization is:

$$1-4\frac{\lambda\Delta t}{\rho c\Delta x^2}\geq 0 \tag{4}$$

$$1-4\frac{\lambda\Delta t}{\rho c\Delta y^2}\geq 0 \tag{5}$$

Considering that the maximum of the actual strip is only 9.6×10^{-2}m along the thickness direction, it becomes meaningless to divide the mesh along the y direction (thickness direction) if the constraints are to be satisfied, so the equations can be simplified to a one-dimensional unsteady differential equation, i.e., mesh only in the x direction (the width of the strip).

In the annealing furnace, the heat exchange between the outside world and the nodes is

$$h=f\cdot S\left[(T_\infty^k)^4-(T_i^k)^4\right]\cdot\Delta y\cdot 1 \tag{6}$$

where S is the Stefan-Boltzmann constant, which is 5. 6697×10^{-8}W/m²·K4. f is the emissivity, which is 0.61W/m²·K according to the field measurements; T_∞^k is the ambient temperature, T_i^k is the surface temperature of the strip, and Δy is the thickness of the strip. According to the Fourier's law of thermal conductivity, the display differential equation for the internal node of heat conduction of a one-dimensional unsteady heat-containing source at moment k can be organized as:

$$\begin{aligned}T_i^{k+1}=&\frac{\lambda\Delta t}{\rho c\Delta x^2}(T_{i-1}^k+T_{i+1}^k-2T_i^k)\\&+2\frac{\Delta t}{\rho c\Delta y}f\cdot S(T_{co}^4-T_i^4)\\&+T_i^k+\frac{\Delta t}{\rho c}H_i\end{aligned} \tag{7}$$

where H_i is the amount of heat brought about by the phase transformation occurring in the time step within the control body, and the enthalpy variable of the transformation from austenite to bainite per unit volume is 5.8×10^{8}J/m³.

Similarly, considering the small value of the thickness of the thin plate strip, the outer wood side of the boundary node can be approximated to be defined as an adiabatic boundary, and the nodal differential equation at the boundary is:

$$\begin{aligned}T_1^{k+1}=&2\frac{\lambda\Delta t}{\rho c\Delta x^2}(T_2^k-T_1^k)\\&+2\frac{\Delta t}{\rho c\Delta y}f\cdot S(T_\infty^4-T_1^4)\\&+T_1^k+\frac{\Delta t}{\rho c}H_1\end{aligned} \tag{8}$$

II. B.Mechanical Performance Test

II. B. 1) Room temperature mechanical properties

The room temperature tensile test is carried out on AGX-50 tensile machine, the tensile specimen is selected according to ASTM metal material tensile test method E8-09 standard, the sample's marking distance is 15mm, the width is 10mm.In order to the accuracy of the experimental results, the experiments are used in the TRViewX type high-precision optical elongation meter to measure the strain in the process of tensile; in order to minimize the contingency of the results of the experiments. At least two tensile tests were conducted in each state. The obtained load divided by the cross-sectional area of the experimental samples is the strength of the material, and the displacement divided by the sample's scale length is the elongation of the material, and the stretching rate during the stretching process is 0.8 mm/min.

Tensile unloading-loading tests were carried out to study the Bauschinger effect on U26Mn2Si2CrNiMo bainitic austenitic steel and to analyze the back stresses and its work hardening behavior. The equipment used for the tests was a ZwickZ050TEW tensile testing machine equipped with a macroXtens extensometer to measure the strain. The parameters of the test, the shape and size of the samples and the preparation method were the same as those of the normal tensile test. From the beginning of the test, after every 1.5% strain, the tensile machine was unloaded at a rate of 180 $Nmin^{-1}$ until the load was reduced to 35 N and then reloaded, and this was repeated 15 times.

II. B. 2) Low temperature mechanical properties

Low-temperature tensile performance test in the INSTRON universal hydraulic servo testing machine to complete, tensile testing machine equipped with a cold box, the use of liquid nitrogen injection to obtain -180 ℃ -0 ℃ low temperature, equipped with a temperature can be measured by the electric coupling, the injection of liquid nitrogen to reach the specified temperature to maintain the tensile test after 3 minutes, due to the limitations of the experimental machine ready to prepare for the experiment of the lowest temperature of this experiment can only be stabilized at -180 ℃. Due to the limitation of the preparation capacity of the experiment machine, the lowest temperature of this low temperature experiment can only be stabilized at -180℃. Tensile test method in accordance with the national standard for low-temperature tensile test methods for metal materials GB/T13239-2006, the sample pitch is 45mm, the width is 10mm.

With EDM wire cutting will be heat-treated specimens along the rolling surface sampling, each process to take two specimens, the specimen to leave a margin of 0.1 ~ 0.2mm. The two flat surfaces of the specimens are ground with a grinder until the wire cutting marks are worn off. The grinding of the side of the tensile specimen is done with sandpaper, and after removing the wire cut traces, the water sandpaper of 200#, 400#, 600# and 800# is used to sand along the tensile direction in order to ensure that there are no large processing traces, so as not to affect the tensile fracture.

Specimen spacing is 45mm, stretching needs to be installed with an extensometer, extensometer inserts aligned with the specimen spacing line, and the extensometer should ensure that the specimen is parallel to the specimen, need to pay attention to: extensometer pulling the pin when the wobble can not be more than 0.015mm, the displacement of the extensometer can not be more than 3mm.

II. C.Microstructural characterization

II. C. 1) Observation by metallurgical microscope (OM)

Using wire cutting from the sample cut 6mm × 5mm size of the small block body specimen, metallographic observation surface selected Normal ND (Normal Direction) and rolling direction RD (Rolling Direction) into the cross-section, metallographic sample preparation and metallographic observation steps are as follows:

(1) cold inlay: the first sample to be inlaid to clean and blow-dry, and according to the mixing ratio: powder/liquid = 5:4 (weight ratio) of the ratio, and then the powder is poured into the cup containing liquid stirred evenly for about 25s in order to mix the formation of a thin paste, will be poured into the mixture of the sample is placed in a cold inlay mold, about 20min after the hardening of inlaid material, from the mold to remove the samples.

(2) rough grinding: the inlaid specimen in 100 #, 300 #, 500 #, 800 #, 1400 #, 1800 #, 2500 # water abrasive sandpaper grinding, replacement of the next sandpaper needs to be the last sandpaper scratches almost abraded, every next sandpaper needs to be turned 90 ° to the specimen to be perpendicular to the last time the scratches, sanding is completed, the specimen surface Basically no deeper scratches.

(3) Polishing: in the metallographic polishing machine on the metallographic specimen for mechanical polishing, the use of particle size of l μm diamond polishing agent, polishing at the same time to observe the surface of the specimen, to be smooth surface without scratching, to achieve a mirror-like effect until.

(4) corrosion: the use of 5% concentration of nitric acid alcohol solution corrosion of the polished surface, corrosion is generally to wait until the surface of the basic loss of metallic luster until the corrosion time in 8 ~ 25s, and then use alcohol to quickly rinse the surface and blow dry.

(5) Metallographic observation: the sample will be moved to the metallographic microscope for tissue observation and analysis, and the metallographic microstructure to take pictures.

II. C. 2) X-ray diffraction (XRD) analysis

An X-ray diffractometer of the X'PERTPRO type was used to analyze the phase composition, quantify the volume fraction of the phases and calculate the total dislocation density in steel. The XRD samples were prepared by electrolytic polishing on the basis of metallographic specimens, in order to avoid the influence of deformation-induced martensite and stress layers on the sample surface that may be generated during grinding of the samples on the XRD test. The electrolytic polishing was carried out using a QJ3005T DC power supply, and the electrolyte was a perchloric acid-glacial acetic acid mixture with a ratio of 1:9. Under the environment of 25℃, the voltage control mode was used, the voltage was 15V, the current was controlled at about 0.5A, and the electrolytic polishing time was about 60s.

II. C. 3) Scanning Electron Microscope (SEM) Observations

The equipment used was an Apreo S LoVac thermal field emission scanning electron microscope from Thermoscientific. Electron channel contrast (ECC) image of backscattered electron signal was used to observe the tissue morphology.

SEM sample preparation process: firstly, rough grinding and mechanical polishing were carried out according to the above metallographic specimen preparation process, and then electrolytic polishing was carried out to reduce or eliminate the surface phase transformation, surface defects and residual stresses generated by grinding. The electrolytic solution is 10% perchloric acid and 90% glacial acetic acid by volume. The parameters of electrolytic polishing are: electrolytic voltage is 20V, electrolytic current is controlled to 0.6A, and electrolytic time is controlled according to the composition of the specimen ranging from 20 to 80s.

II. C. 4) Electron backscatter diffraction (EBSD) observations

The EBSD technique was used to obtain the microstructural information of the materials, and the EBSD experimental data were analyzed using Channel5 commercial software to obtain the phase distribution, weave configuration, grain size size distribution, and stress distribution maps of the materials, as well as the geometrically necessary dislocation densities of the materials based on the crystallographic orientation data of the stress distribution maps. The instruments used were a TESCANMALA3 field emission scanning electron microscope and a NordlysNanoEBSD detector from OXFORD, UK. The test surface was a rolled surface, i.e., RD × TD surface.The EBSD sample preparation process: first, samples were taken from the target state samples, rough ground and mechanically polished according to the metallographic sample preparation process described above, and finally ion etching was performed using an ion etcher model LeicaRES101 with the aim of reducing or eliminating the surface phase transitions, epitaxial defects, and residual stresses produced by grinding. The ion etching voltage was 7kv for 1.5h.

II. C. 5) Transmission Electron Microscopy (TEM) Observations

The observation of microstructure was carried out using a TalosF200XG2 field emission transmission electron microscope. The accelerating voltage was 200 KV. TEM observation method: the sample stage was first tilted, the grains in the field of view were adjusted to the <011>γ grain band axis, and the deformation twins and hexagonal martensite were determined by the TEM bright-field image, dark-field image, and selective electron diffraction in this direction, and the thickness and spacing of deformation twins of the material were statistically analyzed using the TEM bright-field phase, and the hexagonal martensite structure by high-resolution image study. TEM sample preparation process: observation surface selected RD × ND surface, first of all, the sample to be tested in turn using 600 #, 1200 #, 1800 #, 2400 #, 3000 # of sandpaper grinding to a thickness of 35 μm ~ 60 μm, the use of punching device punched out a 2.5 mm diameter small round piece of the sample, and then use the double-jet thinning instrument thinning, electrolysis of double spray the solution used is volume fraction of 10% perchloric acid and 90% glacial acetic acid, and the electrolytic solution was under liquid nitrogen environment.

III. Micromechanical and morphological analysis of U26Mn2Si2CrNiMo bainitic austenitic steel

III. A. Effect of normalizing final cooling temperature on mechanical properties

In order to study the effect of normalizing final cooling temperatures on the microstructure and mechanical properties of the test steels, the final cooling temperatures were set between the temperatures of the bainitic phase transition, which were 320, 335, and 350°C, respectively. The specimens were austenitized at 1000°C for 30 min, and then cooled to the set three normalizing final cooling temperatures by air cooling (about 1°C/s), and finally air cooled to room temperature.

The angular frequency distribution of grain boundary mismatch of the test steels at different final cooling temperatures is shown in Fig. 1(a), in which the proportion of HAGB in the test steels was 50.25% at a final cooling temperature of 350°C. The percentage of HAGB in the test steels at a final cooling temperature of 335°C was 50.25%. When the final cooling temperature is 335°C, the proportion of HAGB in the test steel is 60.17%. At a final cooling temperature of 320°C, the proportion of HAGB in the test steel was 61.06%. The residual austenite grain size distribution is shown in Fig. 1(b). At final cooling temperatures of 335 and 350°C, the test steel has a large amount of residual austenite distributed at grain boundaries or subgranular boundaries, indicating that the bainite phase transformation of the test steel is incomplete at the two final cooling temperatures. When the final cooling temperature is reduced to 320°C, the test steel has no residual austenite.

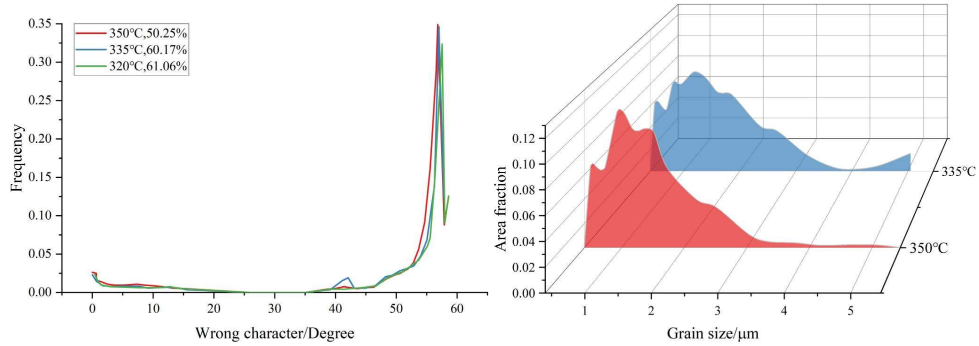

(a) Grain boundary misalignment frequency distribution (b) Grain size distribution of residual austenite

Figure 1: Grain boundaries and residual austenite characteristics

When the final cooling temperature was 320°C, the grain XRD pattern is shown in Figure 2. It can be seen that the microstructure of the metal is fully austenitic, indicating that no phase transformation occurred during the process.

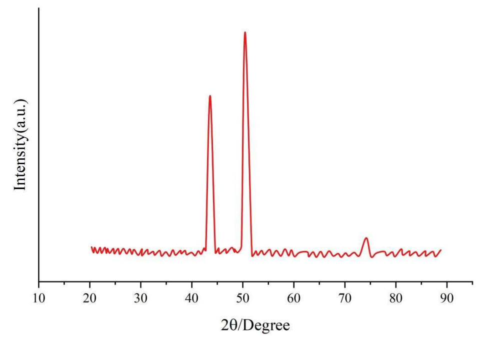

Figure 2: XRD pattern of grains

III. B. Characteristics of the mixture

The number and size of inclusions in the U26Mn2Si2CrNiMo bainitic austenitic steel samples were counted by taking 100 random photographs under SEM at 3000 times using ImageProPlus 6.0 software, and the results are shown in Fig. 3. The average size of inclusions in the H1 sample without added La is about 0.62 μm, and with the increase of La content, the average size of inclusions in the corresponding samples decreases and then increases, but all of them are smaller than the corresponding value of the H1 sample. The number density of inclusions increased from 4958 inclusions/mm² to 6004 inclusions/mm² with increasing La content. In addition, the size of inclusions in the three metal samples is concentrated in the range of less than 0.6 μm, with the H2 sample having the largest proportion of small and medium-sized inclusions, and the proportion of inclusions with a size larger than 1 μm in the H1, H2, and H3 samples is 7.35%, 4.49%, and 4.14%, respectively.

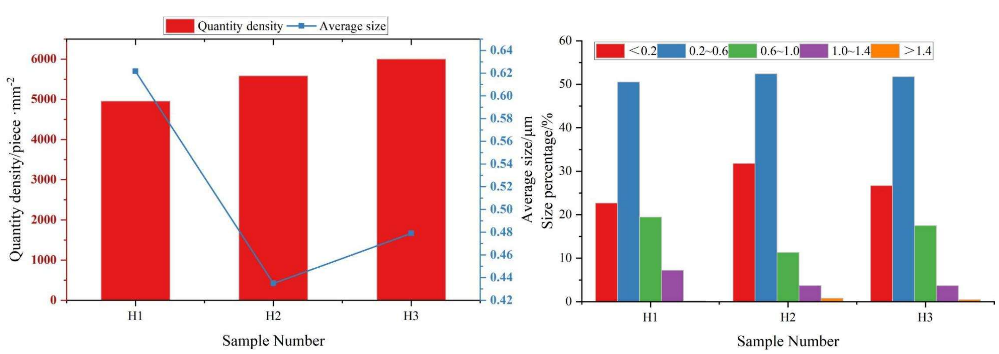

(a) Quantity density and average size (b) Size distribution

Figure 3: Statistical results of the quantity density and size of inclusions

III. C. Mechanism of low temperature tensile properties

III. C. 1) Analysis of low temperature tensile properties

The U26Mn2Si2CrNiMo bainitic austenitic steel in fully annealed state shows significant strength and plasticity enhancement under low-temperature tensile conditions compared with room temperature, while the specimens in cold-rolled state already have high strength at room temperature, and it is worth to expect that their strength and plasticity can be further enhanced under low-temperature conditions. For this reason, room temperature and low-temperature tensile experiments were compared using cold-rolled plates with 85% deformation to verify the low-temperature toughening mechanism of U26Mn2Si2CrNiMo bainitic austenitic steel under high deformation.The engineering stress-strain curves of room-temperature and low-temperature stretching of the cold-rolled plate samples of U26Mn2Si2CrNiMo bainitic austenitic steel, respectively, are shown in Fig. 4. The U26Mn2Si2CrNiMo bainitic austenitic steel cold rolled plate shows very high strength at room temperature tensile, with a yield strength of about 1450 MPa, after which the strength decreases sharply and shows obvious brittleness, and the elongation is relatively low, only about 15%. However, its low-temperature tensile yield strength and tensile strength of strong plasticity performance is extremely excellent. The yield strength exceeds 1750 MPa, the tensile strength exceeds 2000 MPa, and its elongation at break reaches about 60%. Relative to room temperature stretching, its low-temperature tensile properties of strength and plasticity show significant improvement.

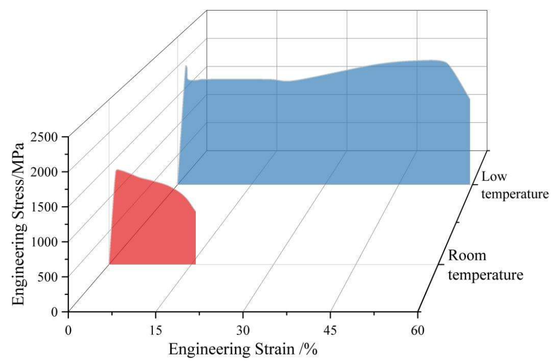

Figure 4: Engineering stress-strain curve

III. C. 2) Effect of Pulsed Current Treatment on Low Temperature Tensile Properties

The engineering stress-strain curves for room-temperature tensile and low-temperature tensile of cold-rolled sheets of U26Mn2Si2CrNiMo bainitic austenitic steel after 10 kV electric pulse treatment are shown in Fig. 5. The trends of room-temperature tensile and low-temperature tensile properties of the 10 kV electropulse-treated sheets are the same as those of the room-temperature tensile and low-temperature tensile properties of the cold-rolled state without the electropulse treatment, with the exception that the 10 kV The yield and tensile strengths of both room temperature tensile and low temperature tensile after electric pulse treatment are slightly lower than those of low temperature tensile without electric pulse treatment. It indicates that softening occurred in the specimens after 10kV electric pulse treatment both at room temperature and low temperature.

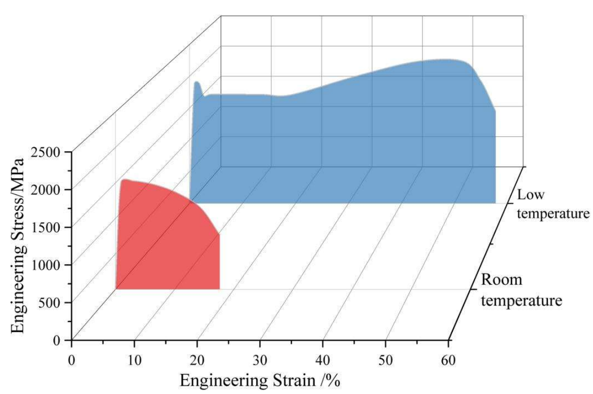

Figure 5: Engineering stress-strain curve

IV. Conclusion

In this paper, for the tensile fracture behavior of U26Mn2Si2CrNiMo bainitic austenitic steel, the key mechanism of inclusions' role is revealed from the dual perspective of micromechanics and morphology evolution, and the following conclusions are obtained.

(1) Effect of temperature on mechanical properties

The normalizing final cooling temperature affects the distribution of grain boundary mismatch angle by controlling the degree of bainite phase transformation, and the fully austenitic organization is achieved under the final cooling condition of 320℃, and the reduction of residual austenite content significantly improves the strength of the material.

(2) Low temperature toughening mechanism

U26Mn2Si2CrNiMo bainitic austenitic steel cold rolled plate at room temperature tensile showed very high strength, yield strength of about 1450MPa, after which the strength falls sharply, showing obvious brittleness, relatively low elongation, only about 15%. However, its low-temperature tensile yield strength and tensile strength of strong plasticity performance is extremely excellent. The yield strength exceeds 1750 MPa, the tensile strength exceeds 2000 MPa, and its elongation at break reaches about 60%. Relative to room temperature stretching, its low-temperature tensile properties of strength and plasticity have shown significant improvement.

(3) Process optimization path

La element addition makes the average size of inclusions first decrease and then increase (H1→H2→H3: 0.62 →0.43→0.49 μm), the number density increases to 6004/mm², and the small-sized inclusions (<0.6 μm) account for more than 70% of the total, which optimizes the efficiency of heterogeneous nucleation; the coarse and large inclusions (>1 μm) are concentrated in the weld region, which becomes the source of crack initiation, leading to the Toughness degradation. Inclusion size control (e.g., adding La to optimize the proportion of small sizes) is the key to improving the overall performance of welded joints.The yield and tensile strengths of room-temperature and low-temperature tensile after 10kV electric pulse treatment were slightly lower than those of low-temperature tensile without electric pulse treatment. This indicates that the softening phenomenon occurred in the specimens after the 10kV electric pulse treatment both at room temperature and low temperature. The experiments show that it is possible to regulate the microstructure and mechanical properties of U26Mn2Si2CrNiMo bainitic austenitic steel under low-temperature conditions by adjusting the pulse intensity.

References

[1] Lin, Y., Yang, H., Ma, L., Li, Z., & Ni, W. (2021). Low-carbon development for the iron and steel industry in China and the world: status quo, future vision, and key actions. Sustainability, 13(22), 12548.

[2] DONG, H., LIAN, X., HU, C., LU, H., PENG, W., ZHAO, H., & XU, D. (2020). High Performance Steels: the Scenario of Theoryand Technology. Acta Metall Sin, 56(4), 558-582.

[3] Ji, Y., Zhu, F., Li, H. X., & Al-Hussein, M. (2017). Construction industrialization in China: current profile and the prediction. Applied Sciences, 7(2), 180.

[4] Wang, M., Liang, X., Ren, W., Tong, S., & Sun, X. (2023). Effect of Mn Content on the Toughness and Plasticity of Hot-Rolled High-Carbon Medium Manganese Steel. Materials, 16(6), 2299.

[5] Niu, G., Zurob, H. S., Misra, R. D. K., Tang, Q., Zhang, Z., Nguyen, M. T., ... & Zou, Y. (2022). Superior fracture toughness in a high-strength austenitic steel with heterogeneous lamellar microstructure. Acta Materialia, 226, 117642.

[6] Wasim, M., Djukic, M. B., & Ngo, T. D. (2021). Influence of hydrogen-enhanced plasticity and decohesion mechanisms of hydrogen embrittlement on the fracture resistance of steel. Engineering Failure Analysis, 123, 105312.

[7] He, S. H., He, B. B., Zhu, K. Y., & Huang, M. X. (2018). Evolution of dislocation density in bainitic steel: Modeling and experiments. Acta Materialia, 149, 46-56.

[8] Hajizad, O., Kumar, A., Li, Z., Petrov, R. H., Sietsma, J., & Dollevoet, R. (2019). Influence of microstructure on mechanical properties of bainitic steels in railway applications. Metals, 9(7), 778.

[9] Królicka, A., Żak, A. M., & Caballero, F. G. (2021). Enhancing technological prospect of nanostructured bainitic steels by the control of thermal stability of austenite. Materials & Design, 211, 110143.

[10] Wang, K., Tan, Z., Gu, K., Gao, B., Gao, G., Misra, R. D. K., & Bai, B. (2017). Effect of deep cryogenic treatment on structure-property relationship in an ultrahigh strength Mn-Si-Cr bainite/martensite multiphase rail steel. Materials Science and Engineering: A, 684, 559-566.

[11] Tian, Y., Tan, Z., Li, H., Gao, B., Zhu, J., Liu, Y., & Zhang, M. (2021). A new finite element model for Mn-Si-Cr bainitic/martensitic product quenching process: Simulation and experimental validation. Journal of Materials Processing Technology, 294, 117137.

[12] Bai, B., Gao, G., Gui, X., Tan, Z., & Weng, Y. (2019). Enhanced mechanical properties of ultrahigh strength Mn–Si–Cr–C steels treated by a novel bainitic transformation plus quenching and partitioning process. Heat Treatment and Surface Engineering, 1(1-2), 63-71.

[13] Qiu, J., Zhang, M., Liu, X., Zhang, X., & Tan, Z. (2020). Characterization of retained austenite in a low carbon high strength Mn–Si–Cr steel. Materials Science and Engineering: A, 797, 139985.

[14] Lemos Bevilaqua, W., Epp, J., Meyer, H., Da Silva Rocha, A., & Roelofs, H. (2020). In situ investigation of the bainitic transformation from deformed austenite during continuous cooling in a low carbon Mn-Si-Cr-Mo steel. Metallurgical and Materials Transactions A, 51, 3627-3637.

[15] Gu, J., Li, D., Liu, S., & Liu, Z. (2024). Microstructure and properties of Mn–Si–Cr alloy steel modified by quenching and partitioning. Materials Testing, 66(3), 305-315.

[16] Zhao, Y. G., Wang, Z., Xu, X. F., Zhang, M. Z., & Jiang, W. Q. (2018). A new preparation technology of structural-gradient materials without a brittle transition zone in a Mn-Si-Cr-B bainitic cast steel. China Foundry, 15, 283-290.

[17] Sun, D., Wang, H., An, X., Wang, G., Huang, S., & Huang, X. (2023). Quantitative evaluation of the contribution of carbide-free bainite, lath martensite, and retained austenite on the mechanical properties of C-Mn-Si high-strength steels. Materials Characterization, 199, 112802.
[18] Zhu, R., Long, X., Zhang, F., Yang, Z., Li, Y., Yang, Y., & Wang, Y. (2025). Optimization of alloying element types and contents in high strength and high toughness bainitic steels. Journal of Materials Research and Technology, 34, 2728-2739.
[19] Yin, B., Han, Y., Wang, W., Li, H., Liu, Y., & Ran, X. (2019). Flow characteristics of a medium–high carbon Mn-Si-Cr alloyed steel at high temperatures. Journal of Materials Engineering and Performance, 28, 5104-5115.